# Nonlinear phenomena, bifurcations, and routes to chaos in an asymmetrically supported rotor–stator contact system

Philip Varney *, Itzhak Green

*Georgia Institute of Technology, Woodruff School of Mechanical Engineering, 801 Ferst Drive, Atlanta, GA 30332, United States*

## ARTICLE INFO

## ABSTRACT

The efficiency of rotating machines can be improved via precisely manufactured bearings with reduced clearances; consequently, the proclivity for rotor–stator contact is increased. A common model used to investigate rotor–stator contact in previous studies is the two degree-of-freedom (DOF) rotor with symmetric support stiffness, where the contact assumes a linear elastic normal restoring force proportional to the rotor–stator interference and a tangential dry Coulomb friction force. Switching between the contacting and non-contacting states creates strong nonlinearity in the equations of motion, and the dynamic response displays a rich profile of behaviors including periodic, quasiperiodic, and chaotic responses via period-doubling, sudden transitions, quasiperiodicity, and intermittency. For the first time, this work emphasizes an asymmetric support stiffness matrix with cross-coupling between the $x$ and $y$ direction stiffnesses. The influence of support asymmetry on the nonlinear rotor response is shown using rotor orbits, frequency spectra, Poincaré sections, and bifurcation diagrams. It is found that the cross-coupling stiffness coefficient $k_{xy}$ has negligible effect on the dynamic response until its magnitude is on the same order as the direct stiffness coefficients. Direct stiffness coefficient asymmetry is shown to affect the rotor's response, where even small asymmetries can qualitatively change the response. Additionally, the importance of including gravity is investigated, and a method is provided for determining the threshold shaft speed above which gravity can be ignored. The dominant route to chaos is period-doubling for the parameters considered here, though other routes to chaos are seen such as a direct transition from periodic to chaotic motion. Finally, observations pertaining to rotor modeling, design, and fault diagnostics are discussed.

© 2014 Elsevier Ltd. All rights reserved.

## 1. Introduction

Increases in turbo-machine efficiency are often achieved via higher operating speeds, lighter shafts, and precisely manufactured bearings with reduced fluid film clearances. Unfortunately, these changes increase susceptibility to faults such as shaft fatigue cracking and rotor–stator contact (i.e., rub). Shaft fatigue cracking is extremely dangerous, though rare; on the other hand, rotor–stator contact often occurs in rotordynamic systems. Contact between the rotor and stator results in decreased machine life via increased wear, heightened susceptibility to fatigue, and adverse thermal effects, in addition to decreased effectiveness of associated fluid-film tribo-elements. Detecting and preventing rotor–stator contact requires detailed knowledge of the conditions leading to and following the onset of contact.

---

* Corresponding author.
  *E-mail addresses:* pvarney3@gatech.edu (P. Varney), itzhak.green@me.gatech.edu (I. Green).

An adept tool for detecting rotordynamic faults and evaluating machinery health is vibration monitoring. Prior to physical implementation, mathematical models of rotor–stator contact are needed to identify hallmark vibration characteristics caused by rub. The first analytical studies investigating rotor–stator contact concerned the appearance of spiral vibrations (i.e., the Newkirk effect) induced by coupled dynamic and thermal effects [1–3]. A simplified analysis of rotor–stator contact as a truncated synchronous response is given by Beatty [4] and Lee and Green [5]. Though intuitive, such a model is incapable of capturing important contact phenomena such as chattering, quasiperiodic responses, and chaotic responses. The first complete nonlinear rotor–stator contact models are given by Beatty [4] and Choy and Padovan [6]. Beatty develops a linear elastic contact stiffness model with dry Coulomb friction, where the interface stiffness generates a normal restoring force. Choy and Padovan use a different approach, where the contact forces are obtained via the rub energy. Transient contact is investigated by suddenly increasing the imbalance once a steady-state non-contacting response is reached; this method reduces the ambiguous nature of initial conditions in the numeric solution. Alternatively, principles of impact and momentum have also been used to model rotor–stator contact [6–10]. Childs [11] models a Jeffcott rotor where the stiffness is fractionally reduced when the rotor's deflection is less than the static deflection.

Still, the linear-elastic/dry friction contact model remains prevalent in current rotor–stator contact modeling [12–29], though various complications have been incorporated. Kim and Noah [12] include a cross-coupling stiffness term, and analyze its influence on the nonlinear system response (as will be discussed shortly). Feng and Zhang [30] analyze velocity perturbations on a non-contacting rotor, showing that such perturbations can induce lingering rubbing contact. In addition, the role of friction in generating backward whirl is prominently discussed. Cao et al. [27] include fractional-order damping in the supports of a rotor–stator contact system. Several authors include nonlinear fluid film force [14,24,31], though the asymmetric nature of the forces is not discussed or emphasized. Static offset between the rotor and the stator is considered by Chavez et al. [32] and Karpenko et al. [20], with gravity and friction being neglected in both analyses. Contact damping has also been included [33,34], with one particular benefit being increased numeric stability in some parameter regimes. Groll and Ewins [34] and Abu-Mahfouz [35] model contact using a Hertzian contact force.

Rotor systems of greater complexity than the Jeffcott rotor are also investigated in the literature. Qin et al. [21,36] use the transfer matrix to obtain the four degree-of-freedom (DOF) equations of motion of a simply supported rotor with an overhung section. Multi-rotor models are occasionally considered [15,19,37–39], though the resulting nonlinear responses are qualitatively similar to those from simple Jeffcott models. Several works consider torsion as a third DOF in a Jeffcott rotor, causing an increased shaft speed range in which chaotic vibrations are seen [16,17]. Stator inertia has also been investigated [24,31,33,40]; most notably, Popprath and Ecker [33] demonstrate that the dynamic response can be dramatically influenced by including the stator mass. Yuan et al. [41] provide a complete 6 DOF rotor model, including lateral, torsional, axial, and angular degrees of freedom, where face contact, rather than annular contact, is considered.

The aforementioned models are strongly nonlinear due to switching between the contacting and non-contacting states; consequently, few analytic solutions are available. Childs [11] uses a perturbation solution where the fractional reduction in stiffness is employed as a small parameter. Kim and Noah [12] use the harmonic balance method (HBM) to predict several periodic solutions, and compare the results to numeric simulation. Lu et al. [10] use a semi-analytic method to obtain periodic solutions of a rub-impact rotor system. However, most studies use numeric integration to extract the system response, with the most popular routines being some variation of the Runge–Kutta algorithm (though other methods have been used such as Newmark-Beta integration [6,21,37,42] or other numeric integration routines [20,28,33]).

The strongly nonlinear nature of rotor–stator contact generates a rich profile of possible responses, including periodic, quasiperiodic, and chaotic behavior. Several of the earliest studies of rotor–stator contact correlated subharmonic and superharmonic oscillations to rub [4,5,11,43,44]. Specifically, Childs [11] uses a perturbation method to explain the appearance of 1/3 and 1/2 subharmonic frequencies. Beatty [4] and Lee and Green [5] show the appearance of integer shaft speed harmonics using a Fourier series analysis of a truncated sine wave. Sawicki et al. [15] discuss the nonlinear nature of the contact model to explain various subharmonic and superharmonic oscillations. Quasiperiodic responses are also caused by rotor–stator contact. Kim and Noah [12] use Floquet theory on periodic solutions obtained with the HBM to show that increasing cross-coupled stiffness causes a secondary Hopf bifurcation, resulting in quasiperiodic responses. The potential for rotor–stator contact to cause chaotic behavior is a dominant aspect of many rotor contact studies [7,8,13,14,20,23, 24,31,33,45], with some of the earliest mentions of chaos being provided by Choi and Noah [45], Li and Païdoussis [9], and Goldman and Muszynska [7]. Lyapunov exponents are used by some authors [9,20,24,31] to quantitatively assess whether the response is periodic, quasiperiodic, or chaotic.

Chaotic behavior has been observed in several nonlinear rotordynamic systems, including rotor–stator contact, unstable hydrodynamic bearings, and pivoted-pad journal bearings [35]. Chaos is reached in dynamical systems via bifurcations from other stable dynamic solutions. The most prevalent routes to chaos in rotor–stator contact systems are period-doubling, sudden transitions, quasiperiodic, and intermittency routes. Period-doubling routes to chaos are encountered in many dynamical systems (most famously by Feigenbaum in the logistic map [46]). Each subsequent bifurcation results in the response instantaneously transitioning from period-$k$ motion to period-$2k$ motion. The bifurcations occur more and more frequently, eventually resulting in chaos. In rotor–stator contact, period-doubling routes to chaos are observed in bifurcations using shaft speed [14,21,24,25,35,47], friction coefficient [9], and imbalance [14] as control parameters. Routes to chaos other than period-doubling are also seen, including the quasiperiodic route [9,14,18] and intermittency [14]. Chu and Zhang [14] present a thorough study of nonlinear responses in a Jeffcott rotor supported by fluid-film bearings with rotor–stator contact; periodic, quasiperiodic, and chaotic responses are observed for many parameter combinations.

Bifurcations involving shaft speed, damping ratio, and imbalance are provided to study routes to chaos. When the damping ratio is used as the control parameter, intermittency mechanisms bifurcate the system into chaotic behavior. Grazing bifurcations, where the rotor grazes the stator with zero normal velocity, are witnessed in rotor–stator contact systems, causing period doubling, quasiperiodic responses, and chaos [10,32,36]. Chavez et al. [32] develop an analytic curve to determine the onset of grazing bifurcations, though gravity and friction are neglected. Bifurcation studies using other control parameters are given, including parameters such as shaft speed [13,15,16,20,23,33,44], damping ratio [20,23], imbalance [23], torsional stiffness [16], clearance [28], contact stiffness [20,23], friction coefficient [23], and stator mass [33]. Other phenomena can be seen in rotor–stator contact systems, such as backward whirl, whip, and full reverse rub [40,48–50], though these phenomena are not emphasized in this study.

Several studies suggest methods and procedures for realistically diagnosing rub. Yu [50] provides several case studies of real turbomachines experiencing rub, emphasizing the use of superharmonic oscillations and backward whirl for diagnosing rotor–stator contact. Sawicki et al. [15] discuss the use of chaos mapping for rub diagnostics. Chu and Lu [19] diagnose the location of rotor–stator contact in a multi-rotor system using a linear least squares approach on the rotor stiffening effect. Full spectrum analysis, which separates each harmonic into its constituent forward and backward components, is also used for rub diagnosis [50–54]. Time–frequency–energy signal processing techniques such as reassigned scalograms, wavelets, and the empirical mode decomposition/Hilbert–Huang transform can localize rub temporally [22,29,55,56]. Abu-Mahfouz and Amit Banerjee [28] describe three evolutionary algorithms (particle swarm optimization, differential evolution, and the firefly algorithm) to identify rotor–stator contact parameters from quasiperiodic and chaotic responses.

The purpose of this work is to investigate nonlinear phenomena, bifurcations, and routes to chaos in an asymmetrically supported rotor. Here, the shaft flexibility is assumed to be much greater than the support stiffness, and is therefore negated in the analysis (future works will address shaft flexibility and gyroscopic effects). Though some studies have concerned fluid film forces, which are generally asymmetric, the results have focused on support nonlinearity rather than asymmetry. Beyond fluid-film effects, support asymmetry can be caused by unequally worn rolling element bearings, journal bearings, or other similar damage. Here, for the first time, support asymmetry is emphasized and its influence on the nonlinear system response determined. Many studies neglect gravity in their analyses [6,9,17,18,20,23,30,32] without justification. However, the nonlinearity precludes linear superposition and necessitates the inclusion of gravity. Thus, a subsidiary goal here is to establish guidelines for when gravity must be included or can be negated. To accomplish these goals, a two DOF rotor model with external asymmetric supports is used with a linear elastic/dry friction contact model, and the equations of motion are solved numerically. Results are interpreted using waveforms, rotor orbits, frequency spectra, Poincaré sections and bifurcation diagrams.

## 2. Rotordynamic modeling

Consider the externally supported rotor shown in Fig. 1, where the support stiffnesses are defined in the inertial *xyz* reference frame (where axis *x* is coming out of the page). When only cylindrical modes are considered (here, shaft flexibility and conical modes are not considered), the rotor's position is uniquely described by two degrees of freedom $u_x$ and $u_y$, chosen as the deflection of the rotor's geometric center *C* referenced from the undeflected position of the rotor *O*. For a shaft rotating with frequency *n*, the well-known equations of motion [57] including a rotating imbalance and gravity (without contact) are

$$m\ddot{u}_x + c\dot{u}_x + k_{xx}u_x + k_{xy}u_y = m\epsilon n^2 \cos(nt) \tag{1}$$

$$m\ddot{u}_y + c\dot{u}_y + k_{yy}u_y + k_{yx}u_x = m\epsilon n^2 \sin(nt) - mg \tag{2}$$

where the rotor's mass is *m*, the viscous damping coefficient is *c*, and $k_{ij}$ is the stiffness coefficient relating a force in the *j*th direction to a displacement in the *i*th direction. Here, it will be assumed that $k_{xy} = k_{yx}$. The rotor's center of mass is offset from the geometric center by the eccentricity $\epsilon$. The rotor is constrained within a stationary housing (i.e., the stator) with clearance $\delta$. Contact occurs when the rotor's radial deflection $r = \sqrt{u_x^2 + u_y^2}$ exceeds the clearance. The undeflected rotor of radius *R* is shown in Fig. 2a, where the rotor's geometric center *C* is initially located at the undeflected location *O*. When
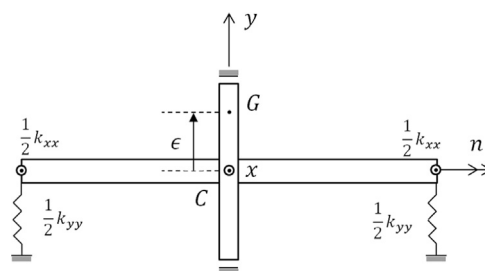


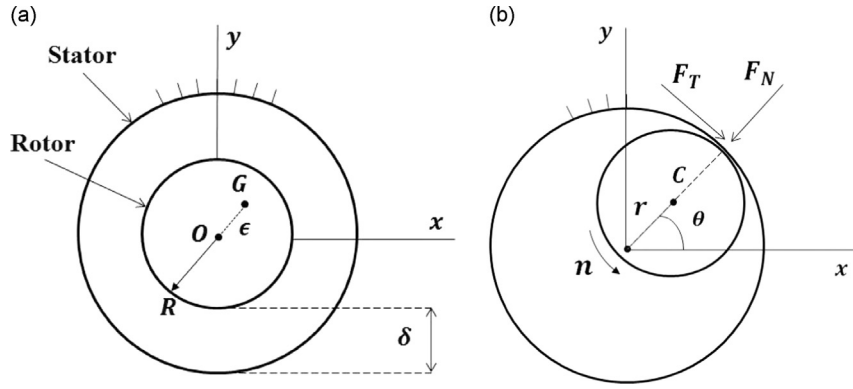**Fig. 1.** Asymmetrically supported rotor with stator clearance.

**Fig. 2.** Lateral contact in the overhung rotordynamic system. (a) Undeflected rotor and (b) deflected rotor with lateral contact.

contact occurs (that is, when $r > \delta$), an elastic-normal restoring force $F_N$ and a tangential friction force $F_T$ are generated at the rotor–stator interface (see Fig. 2b). The elastic restoring force is linearly proportional to the interference between the rotor and the stator by the contact stiffness $k_c$, while the tangential friction force is proportional to the normal force by the friction coefficient $\mu$:

$$F_N = \begin{cases} 0, & r < \delta \\ k_c(r-\delta)h(r-\delta), & r > \delta \end{cases} \tag{3}$$

$$F_T = \mu F_N \tag{4}$$

The Heaviside function $h(r-\delta)$ is used to ensure contact forces are only developed when the rotor's deflection exceeds the clearance. It is well known that the direction of the friction force can vary according to the direction of the rotor–stator contact point's velocity. However, such a condition was not observed to influence the results here due to the chosen system parameters and high shaft speeds. Thus, in this work the direction of the friction force will be assumed constant in the negative tangential direction as per Fig. 2b. Recognizing that

$$\cos\theta = \frac{u_x}{r}, \quad \sin\theta = \frac{u_y}{r}, \tag{5}$$

and referencing Fig. 2b, the contact forces are decomposed into the $x$ and $y$ inertial directions:

$$F_x = F_T \sin\theta - F_N \cos\theta \tag{6}$$

$$F_y = -F_T \cos\theta - F_N \sin\theta \tag{7}$$

Taking into account Eqs. (3)–(5), the total contact force $F_C$ is projected onto the $x$ and $y$ inertial directions:

$$F_{Cx} = k_c \frac{r-\delta}{r}(\mu u_y - u_x)h(r-\delta) \tag{8}$$

$$F_{Cy} = k_c \frac{r-\delta}{r}(-u_y - \mu u_x)h(r-\delta) \tag{9}$$

Including contact forces, the equations of motion of the asymmetrically supported rotor are the following:

$$m\ddot{u}_x + c\dot{u}_x + k_{xx}u_x + k_{xy}u_y + k_c\frac{r-\delta}{r}(u_x - \mu u_y)h(r-\delta) = m\epsilon n^2 \cos(nt) \tag{10}$$

$$m\ddot{u}_y + c\dot{u}_y + k_{yy}u_y + k_{xy}u_x + k_c\frac{r-\delta}{r}(u_y + \mu u_x)h(r-\delta) = m\epsilon n^2 \sin(nt) - mg. \tag{11}$$

The equations of motion are a non-autonomous system of coupled, nonlinear second-order differential equations where the dominant driving frequency is the shaft speed $n$. This hybrid dynamical system [32,58] alternates between the linear non-contacting state and the nonlinear contact state, where the switching behavior is a strong nonlinearity, precluding the ability to obtain closed-form solutions.

Time is non-dimensionalized such that $\tau = nt$; this transformation eases the numeric solution and allows for easy comparison between the responses at different shaft speeds. Additionally, non-dimensionalization of time by the shaft speed $n$ results in a non-dimensionalization of the frequency content such that the synchronous component always occurs at unity. Defining derivatives with respect to $\tau$ by $(\bullet)'$ and dividing by $mn^2$ yield the following mass-normalized form of

Eqs. (10) and (11):

$$u_x'' + \frac{2\zeta\overline{\omega}_n}{n}u_x' + \frac{\omega_{xx}^2}{n^2}u_x + \frac{\omega_{xy}^2}{n^2}u_y + \frac{\omega_c^2}{n^2}\frac{r-\delta}{r}(u_x - \mu u_y)h(r-\delta) = \epsilon\,\cos\,\tau \tag{12}$$

$$u_y'' + \frac{2\zeta\overline{\omega}_n}{n}u_y' + \frac{\omega_{yy}^2}{n^2}u_y + \frac{\omega_{xy}^2}{n^2}u_x + \frac{\omega_c^2}{n^2}\frac{r-\delta}{r}(u_y + \mu u_x)h(r-\delta) = \epsilon\,\sin\,\tau - \frac{g}{n^2}. \tag{13}$$

where $\omega_{ij}^2 = k_{ij}/m$ and $\overline{\omega}_n = 1/2(\omega_{xx} + \omega_{yy})$. Damping is normalized such that $c/m = 2\zeta\overline{\omega}_n$, where $\zeta$ is defined to be the mean damping ratio; if $\overline{\omega}_n$ and $c$ are already determined, the mean damping ratio can provide a relative estimation of the effect of damping. The contact stiffness is redefined as $\omega_c^2 = k_c/m$. Prior to numeric integration, the equations of motion must be placed in the state space. The state vector is defined in the extended phase space as

$$S := (u_x, u_x', u_y, u_y', \tau) \in \mathbb{R}^4 \times \mathbb{S}^1$$
$$:= (x_1, x_2, x_3, x_4, \tau) \in \mathbb{R}^4 \times \mathbb{S}^1 \tag{14}$$

while the system parameters are

$$P := (n, k_{xx}, k_{yy}, k_{xy}, k_c, \epsilon, \delta, \mu, c) \in \mathbb{M}^9 \times \mathbb{S}^1 \tag{15}$$

Reorganizing Eqs. (12) and (13) into a set of four first-order differential equations according to the state vector in Eq. (14) gives

$$\begin{Bmatrix} x_1' \\ x_2' \\ x_3' \\ x_4' \end{Bmatrix} = \frac{1}{n^2}\begin{bmatrix} 0 & 1 & 0 & 0 \\ -\omega_{xx}^2 - \phi_L & -2\zeta\overline{\omega}n & \mu\phi_L - \omega_{xy}^2 & 0 \\ 0 & 0 & 0 & 1 \\ -\mu\phi_L - \omega_{xy}^2 & 0 & -\omega_{yy}^2 - \phi_L & -2\zeta\overline{\omega}n \end{bmatrix}\begin{Bmatrix} x_1 \\ x_2 \\ x_3 \\ x_4 \end{Bmatrix} + \begin{Bmatrix} 0 \\ \epsilon\,\cos\,\tau \\ 0 \\ \epsilon\,\sin\,\tau - g/n^2 \end{Bmatrix}, \tag{16}$$

where

$$\phi_L = \omega_c^2 \frac{r-\delta}{r}h(r-\delta) \tag{17}$$

The equations are now in a state-space form suitable for numeric integration.

## 3. Results

The equations of motion are integrated numerically using MATLAB ®'s hybrid fourth/fifth-order variable-step Runge–Kutta solver, ode45. The numeric stiffness of the equations was evaluated by comparing the solution time to that obtained using the stiff solver ode23s. The stiff solver resulted in substantially greater solution times than ode45, indicating that the system is non-stiff and justifying the use of ode45. To extract only the steady-state response, the solution was carried out to 500 periods of the non-dimensional forcing frequency (i.e., $1000\pi$ non-dimensional units of time) for high values of damping and 1500 periods for low values of damping. The time ranges of the waveforms presented in the following sections all reside in the steady-state regime. Additionally, the importance of selecting appropriate error tolerances is imperative due to small rotor–stator interferences. The relative tolerance was set to $10^{-9}$ while the absolute tolerance was set to $10^{-13}$. These values were selected by progressively increasing the tolerance until (a) convergence was obtained and (b) the frequency spectrum showed no evidence of noise in numeric solutions. The rotor's static deflection is used as the initial condition in each case, with zero initial velocity; the system is then set into motion via the non-autonomous terms in Eq. (16). Parameter sets used to generate specific results are referenced and indicated in Appendix A.

### 3.1. Periodic, quasiperiodic, and chaotic responses

Nonlinear dynamic systems are capable of a vast array of qualitatively different responses. The nature of solutions to linear systems are understood a priori; the output assumes a scaled form of the input, and linear superposition holds. However, the same cannot be said concerning nonlinear systems. In linear systems, quantitative changes in system parameters give quantitative changes in the response. In nonlinear systems, changes in parameters can result in bifurcation phenomena, generating responses which are qualitatively different from those encountered in other, often nearby, parameter ranges. The purpose here is to demonstrate that rotor–stator contact systems result in a plethora of responses, including periodic, quasiperiodic, and chaotic dynamics responses. Since the objective here is only to demonstrate the wide variety of possible nonlinear responses in a simple rotor model, support asymmetry is only temporarily neglected ($k_{xx} = k_{yy} = k, k_{xy} = 0$).

Responses are presented using waveforms, rotor orbits, frequency spectra, and Poincaré sections. In conventional nonlinear dynamics terminology, an orbit is a projection of the entire solution $\mathbf{x}(t) \in \mathbb{R}^n \times \mathbb{S}^1$ unto the $n$-dimensional phase space. Such a representation removes the time-evolution of the response but retains the nature of the solution. Here, as is typical in rotordynamics, the orbit is taken to be the trace of the rotor's geometric center rather than the full solution $\mathbf{x}(t)$. The waveforms are time responses of a specified degree of freedom demonstrating the evolution of one state space variable

versus time. For periodic solutions, the waveforms repeat with time. However, it is very difficult to ascertain the exact nature of the solution from only the waveform (especially for other dynamic responses such as quasiperiodic and chaotic responses). Further information is gleaned from the frequency spectra of each DOF. This information is very useful, as rotordynamic condition monitoring systems often rely on shaft speed subharmonics and superharmonics for fault detection and diagnosis. Poincaré sections provide a qualitative assessment of the dynamic response. Specifically, a Poincaré section $\Sigma$ is a hyper-surface in the state space that is transverse to the dynamical system's flow. In a non-autonomous system with excitation period $T$, 'transverse to the flow' implies that the solution $\mathbf{x}(t)$ is sampled every $T$ seconds. Since Eq. (16) has been normalized with respect to the forcing frequency $n$, the Poincaré section is obtained by sampling the response every $2\pi$ non-dimensional units of time (i.e., once per rotor revolution), thus supplying a stroboscopic picture of the system's evolution. Also, since $\mathbf{S} \in \mathbb{R}^4 \times \mathbb{S}^1$, a reduced Poincaré section $\Sigma_r$ is used where the reduced state space $\mathbf{S}_r := (u_x, u_y) = (x_1, x_3) \in \mathbb{R}^2 \times \mathbb{S}^1$ is sampled. These sampled points are referred to as Poincaré return points (and, as will be seen later, a plot of the Poincaré return points versus a specified control parameter gives a bifurcation diagram).

### 3.1.1. Periodic responses

Nayfeh and Balachandran [59] define a periodic solution of least-period $T$ as a solution for which if $\mathbf{x} = \mathbf{x}_0$ at $t = t_0$, then $\mathbf{x}(\mathbf{x}_0; t_0) = \mathbf{x}(\mathbf{x}_0; t_0 + T)$. The number of the periodic response is determined by the number of unique Poincaré return points; for a period-$k$ response, $k$ unique return points are observed. The waveform repeats over time at the lowest period of the system, while the orbit commensurately traces an identically repeated closed loop. In the frequency domain, a period-$k$ response contains $k$ frequencies between each integer harmonic of the fundamental forcing frequency (in this case, the shaft speed $n$). For example, a period-3 response has harmonics 1/3, 2/3, 1, 4/3, 5/3, 2, etc., while a period-2 response has harmonics 1/2, 1, 3/2, 2, etc.

A wide variety of periodic responses are observed upon solving Eq. (16) for various parameter combinations and shaft speeds. Figs. 3–6 show several possible periodic responses obtained from parameter set 1 (see Table A1 in Appendix A), using various damping ratios at a constant shaft speed $n = 1.54\omega_n$ (where $\omega_n = \sqrt{k/m}$). The dashed line in each waveform represents the threshold deflection above which contact occurs ($r/\delta = 1$); this clearance is also shown in the rotor orbit as a dark circle. The Poincaré section is duplicated in each orbit plot for clarity.

A gravity-dominated period-1 response is shown in Fig. 3, where the orbit resides primarily in the lower half of the clearance (see Fig. 3b). The rotor contacts the lower portion of the stator three times per revolution, resulting in chattering behavior in the waveform (Fig. 3a). This chattering is approximated by several authors using a simple truncated sine wave [4,5]. The period-1 motion generates only integer shaft speed harmonics, as corroborated by Beatty [4] and Lee and Green
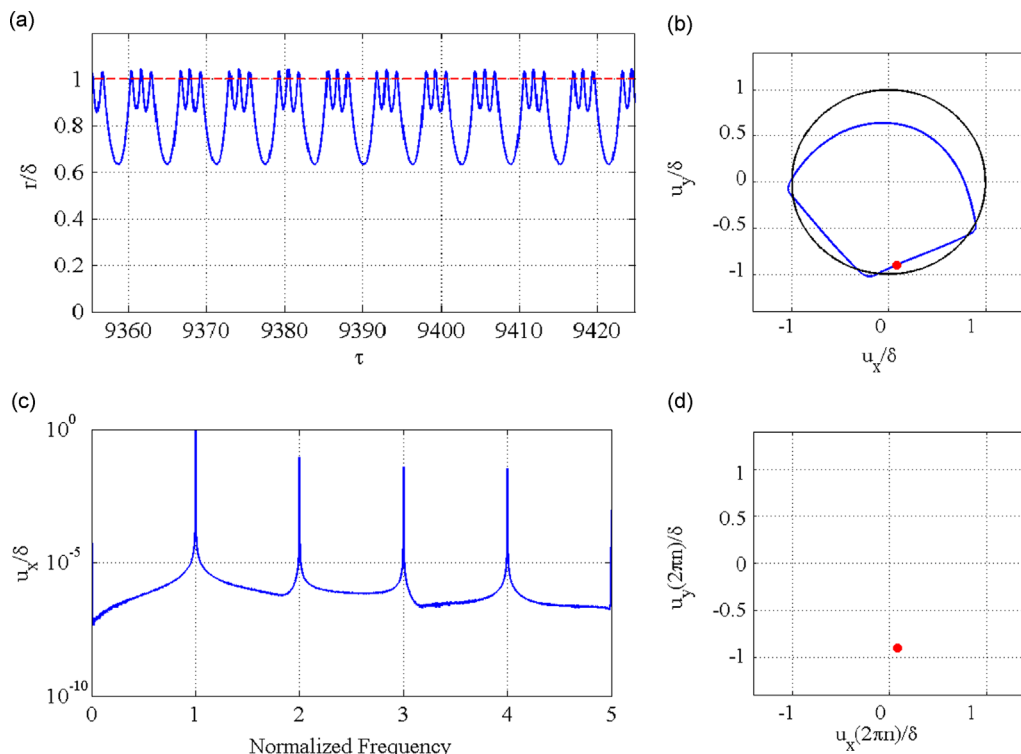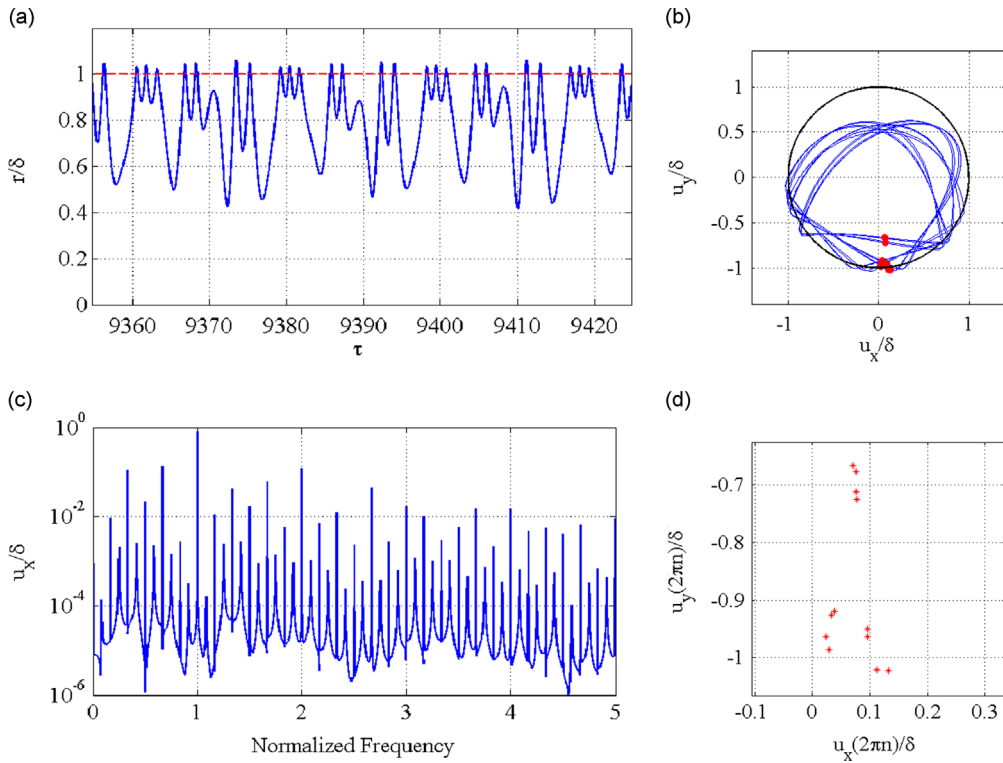


Fig. 3. Period-1 response (symmetric rotor parameter set 1, $n = 1.54\omega_n$, $c = 3943.6$ N s/m ($\zeta = 0.36$)). (a) Waveform (steady state), (b) orbit, (c) frequency spectrum, and (d) Poincaré section.
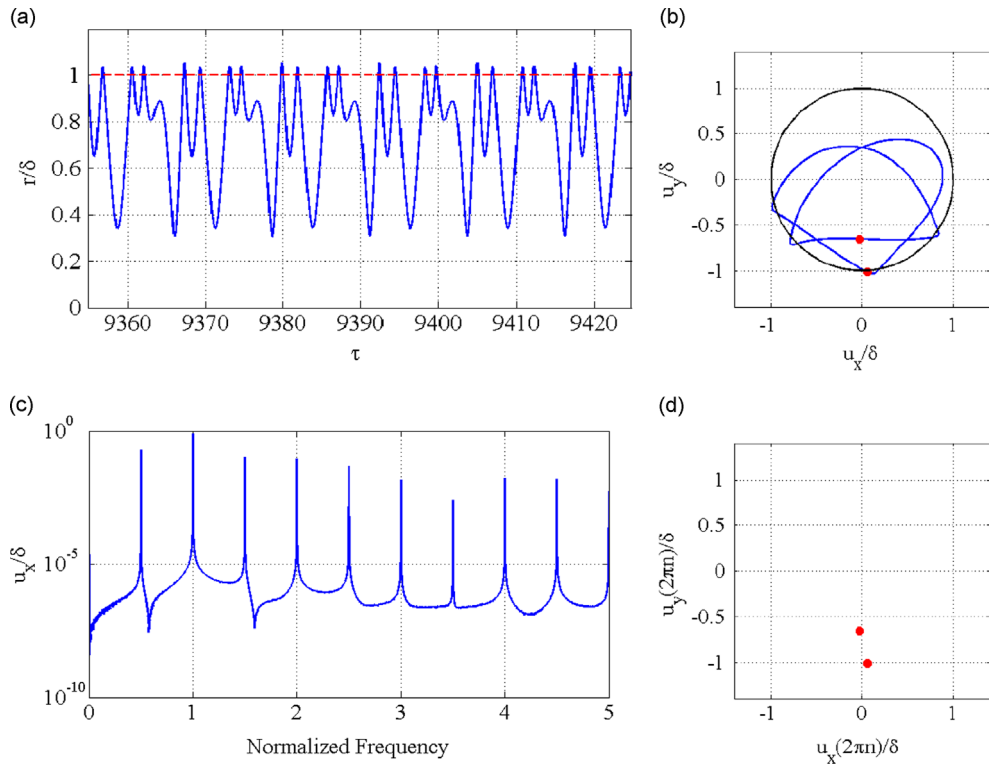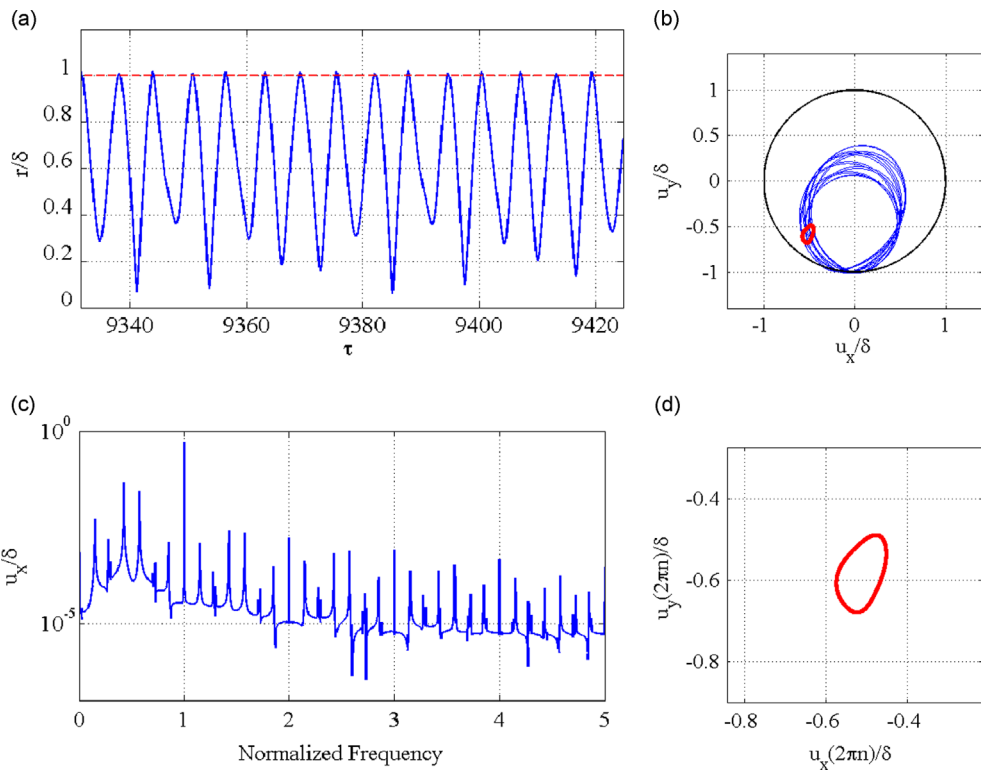
**Fig. 4.** Period-2 response (symmetric rotor parameter set 1, $n = 1.54\omega_n$, $c = 4820.0$ N s/m ($\zeta = 0.44$)). (a) Waveform (steady state), (b) orbit, (c) frequency spectrum, and (d) Poincaré section.
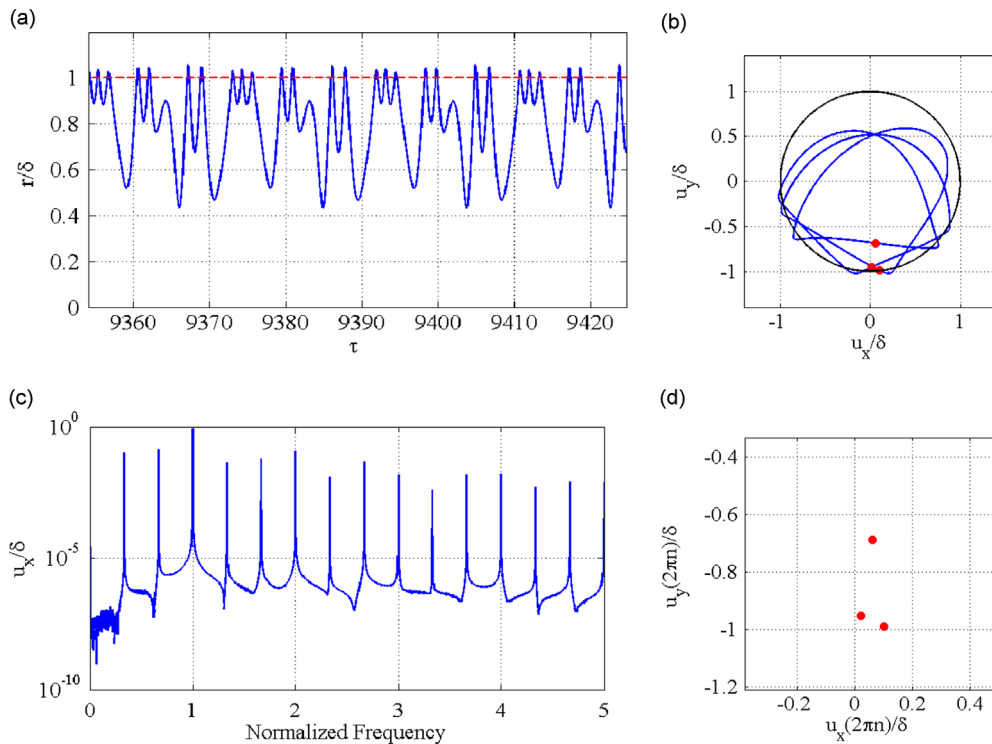


**Fig. 5.** Period-3 response (symmetric rotor parameter set 1, $n = 1.54\omega_n$, $c = 4381.8$ N s/m ($\zeta = 0.4$)). (a) Waveform (steady state), (b) orbit, (c) frequency spectrum, and (d) Poincaré section.
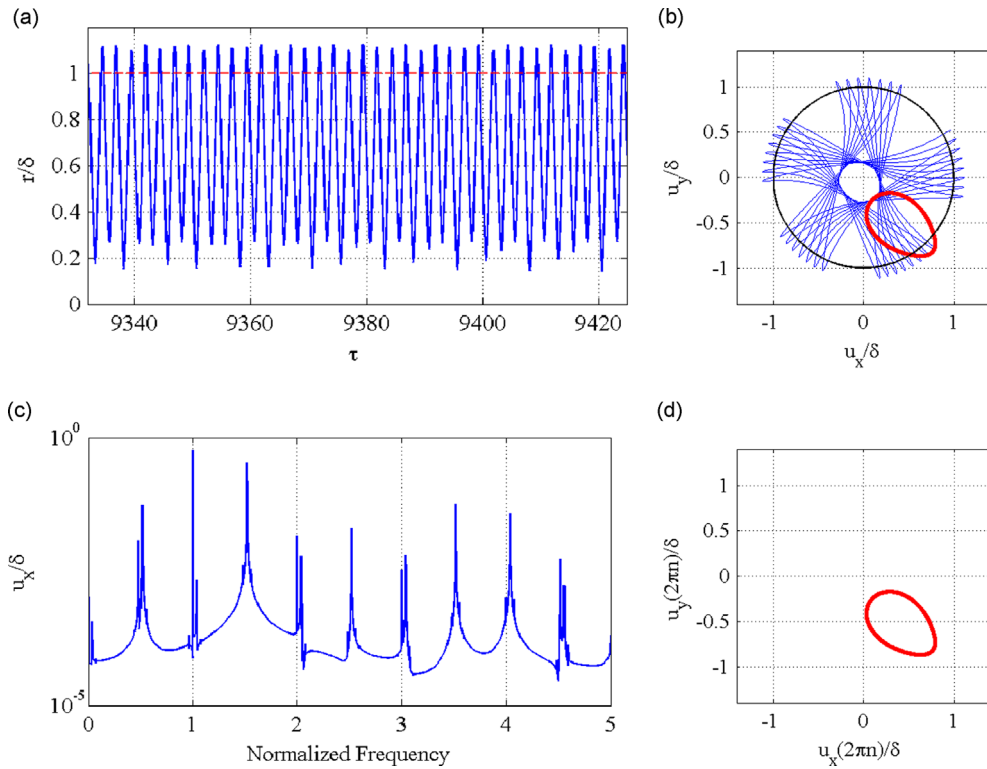
**Fig. 6.** Period-12 response (symmetric rotor parameter set 1, $n = 1.54\omega_n$, $c = 4321.5$ N s/m ($\zeta = 0.3945$)). (a) Waveform (steady state), (b) orbit, (c) frequency spectrum, and (d) Poincaré section.
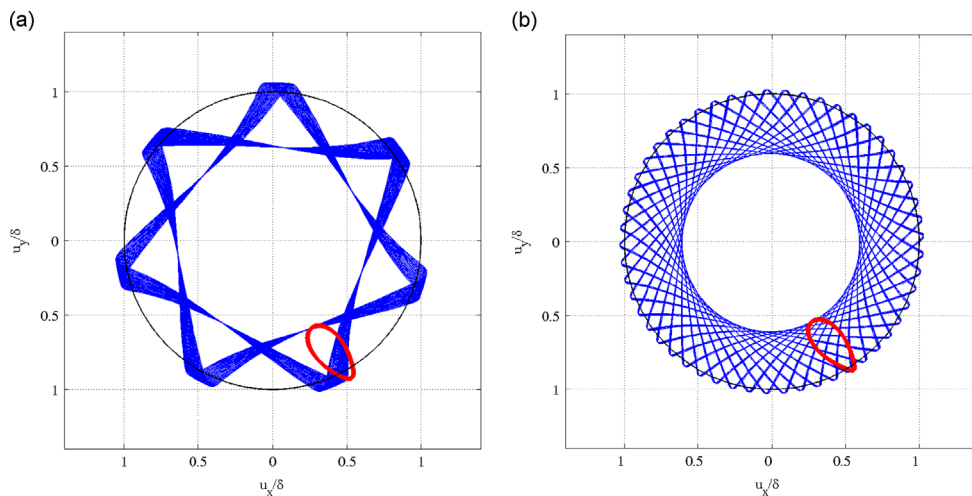


**Fig. 7.** Quasiperiodic response (symmetric rotor parameter set 3, $n = 2.25\omega_n$). (a) Waveform (steady state), (b) orbit, (c) frequency spectrum, and (d) Poincaré section.
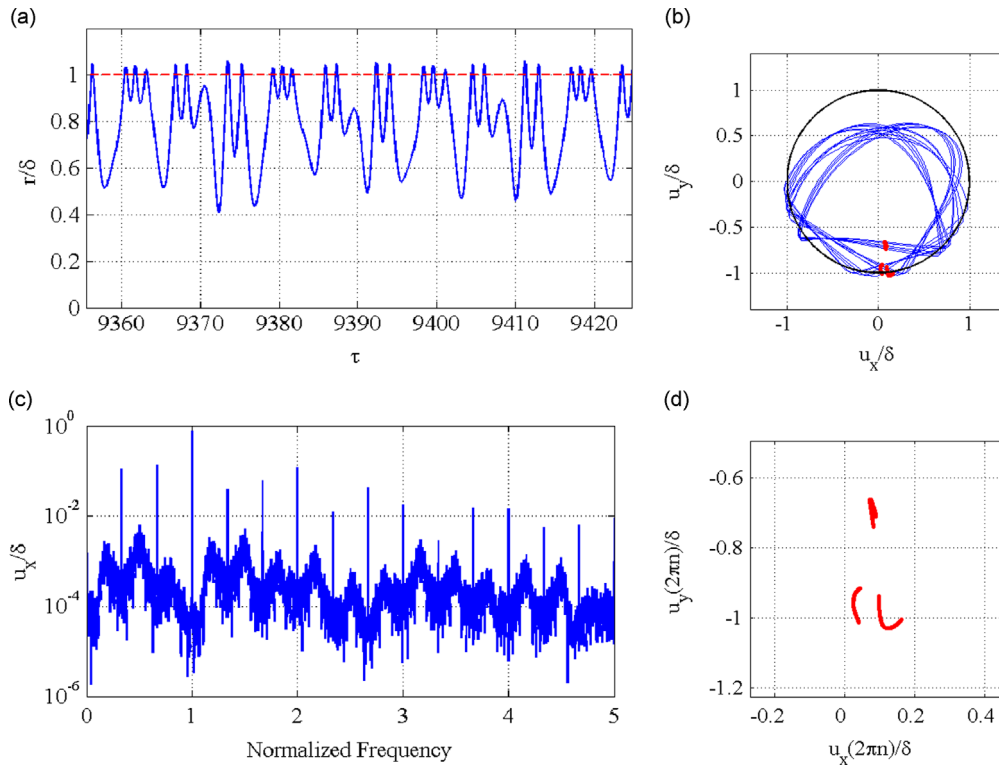
**Fig. 8.** Quasiperiodic response (symmetric rotor parameter set 3, $n = 2.41\omega_n$). (a) Waveform (steady state), (b) orbit, (c) frequency spectrum, and (d) Poincaré section.



**Fig. 9.** Quasiperiodic responses (symmetric rotor parameter set 6, $n = 2.5\omega_n$). (a) $\sqrt{k_c/k} = 32.34$ and (b) $\sqrt{k_c/k} = 66.67$.

[5] in their simple sinusoidal truncation models. A plethora of other period responses can be found using other parameter combinations; here, only period-2 , period-3, and period-12 responses are shown for brevity (Figs. 4, 5, and 6, respectively). As the period number increases, additional Poincaré return points appear, along with non-integer harmonics in the frequency spectra. For example, the period-2 response in Fig. 4 contains two unique Poincaré return points. On the rotor's orbit and waveform, this manifests as an alternation between two distinct rotor motions (analogous conclusions can be drawn concerning the period-3 and period-12 responses in Figs. 5 and 6). Chattering behavior induced by a gravity-dominated response is seen in each waveform, becoming more complex with increasing period number.

**Fig. 10.** Chaotic response (symmetric rotor parameter set 1, $n = 1.54\omega_n$, $c = 4309.5$ N s/m ($\zeta = 0.3934$)). (a) Waveform (steady state), (b) orbit, (c) frequency spectrum, and (d) Poincaré section.

### 3.1.2. Quasiperiodic responses

Nayfeh and Balachandran [59], Hale [60], and Urabe [61] rigorously define quasiperiodic solutions. Here, quasiperiodic solution is recognized by (a) incommensurate frequency content (i.e., the ratio of peaks is irrational) and (b) closed loops in Poincaré section. A convenient description of quasiperiodic motion is toroidal motion. The solution 'travels' along the inside perimeter of the torus, and the Poincaré section records the rotor's position as it passes a certain location (or slice) of the torus. In a period-$k$ response, the solution passes only through $k$ locations on the torus cross-section perimeter; for a quasiperiodic response, the solution traces out the interior perimeter. Several representative quasiperiodic responses are shown in Figs. 7–9 for a symmetrically supported rotor. Note that in each case, the Poincaré section is a closed loop, and the frequency spectra contain incommensurate frequencies. The quasiperiodic response in Fig. 7 is dominated by gravity, while the responses in Figs. 8 and 9 are dominated by inertial effects.
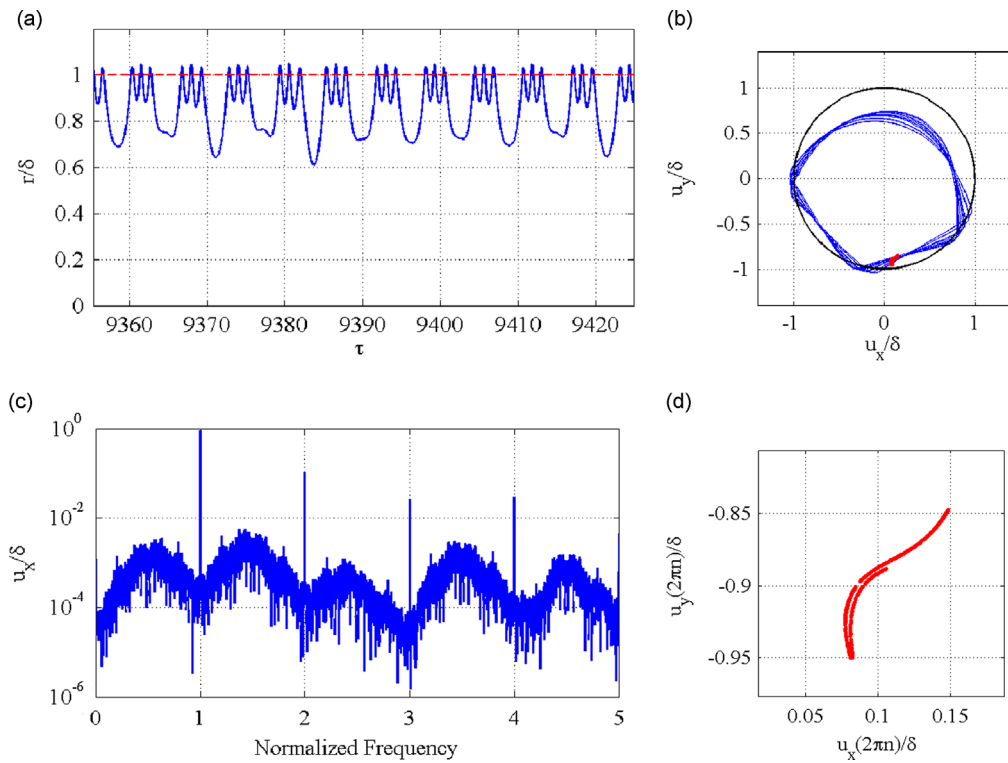
### 3.1.3. Chaotic responses

As discussed previously, rotor–stator contact systems are susceptible to aperiodic/chaotic behavior. Whereas periodic and quasiperiodic responses have defined peaks in the frequency domain and a clear structure in the Poincaré section, chaotic responses display broad-band frequency content and complicated or fractal Poincaré sections. Nayfeh and Balachandran [59] give a detailed discussion of chaos; here, chaotic and/or aperiodic responses are identified by broadband frequency content and complex Poincaré sections.

Rotordynamic chaotic responses often include frequency modulation; several frequency-modulated chaotic responses are shown in Figs. 10 and 12, where the frequency modulation can be heuristically correlated to Poincaré section structure. In Fig. 10, frequency modulation is seen at normalized frequencies of $j/3$, where $j = 0, 1, 2, \ldots$. Correspondingly, the Poincaré section contains three unique components, signifying the presence of a period-3 unstable ghost attractor in the response. The same phenomena are also visible in Figs. 11 and 12, but for period-1 and period-2 ghost attractors, respectively. Other chaotic responses display less frequency modulation; such a case is provided for an asymmetrically supported rotor in Fig. 13, where the magnitude of the broadband character is beginning to approach that of the dominant shaft speed harmonics. Consequently, the Poincaré section displays less structure than those in Figs. 10–12.

### 3.2. Influence of gravity

Many rotor–stator contact studies neglect gravity without sufficient justification [6,9,17,18,20,23,30,32]. Except in the case of vertical shafts, neglecting gravity can be a major issue when analyzing nonlinear rotor systems; here, physical

**Fig. 11.** Chaotic response (symmetric rotor parameter set 4, $n = 1.545\omega_n$). (a) Waveform (steady state), (b) orbit, (c) frequency spectrum, and (d) Poincaré section.
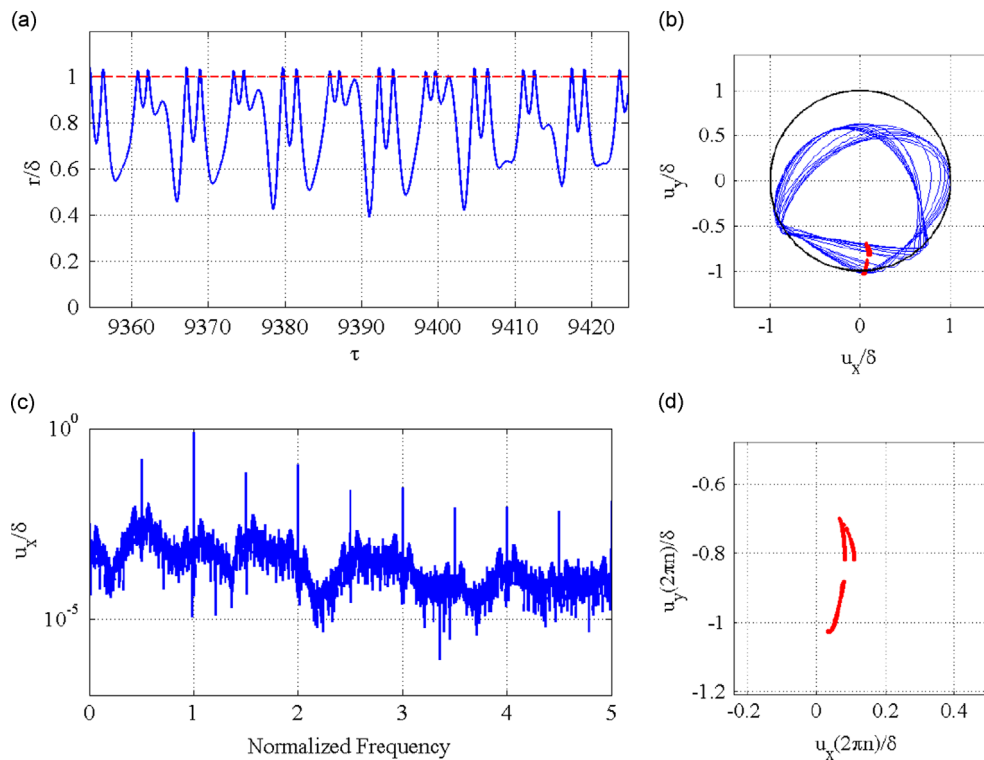


**Fig. 12.** Chaotic response (symmetric rotor parameter set 3, $n = 1.34\omega_n$). (a) Waveform (steady state), (b) orbit, (c) frequency spectrum, and (d) Poincaré section.
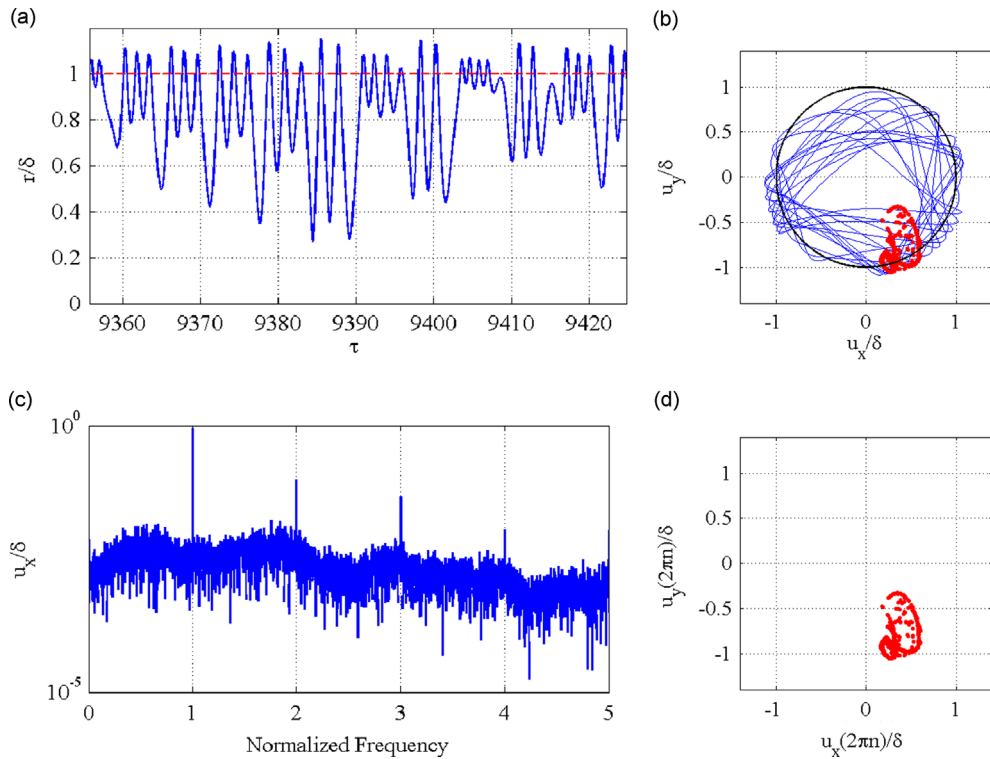
**Fig. 13.** Chaotic response in an asymmetric system (asym. parameter set 2, $n = 2.0\overline{\omega}_n$). (a) Waveform (steady state), (b) orbit, (c) frequency spectrum, and (d) Poincaré section.
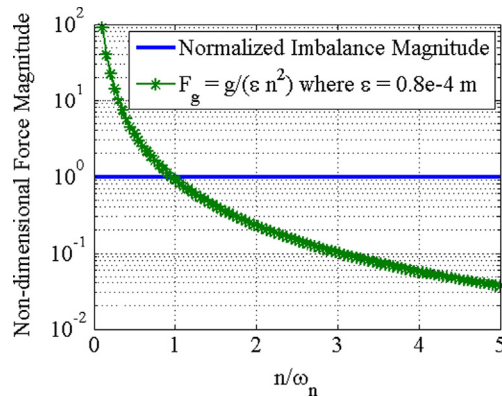


**Fig. 14.** Influence of gravity, where $\epsilon = 0.8(10)^{-4}$ m.

intuition is used to understand the nonlinearity's interaction with gravity. In linear systems, the principle of superposition holds: if the rotor's response to both imbalance and gravity is sought, each response is found independently and summed to generate the total response. Physically, this is equivalent to shifting every point on the synchronous circular orbit down by the rotor's static deflection. Such a shift is impossible if a clearance exists between the rotor and the stator that is smaller than the sum of the static deflection and imbalance response; the stator constrains the rotor, giving a response which is qualitatively different than that which would be obtained via superposition. Thus, gravity must generally be considered to obtain accurate and realistic results for horizontal rotor–stator contact systems.

Observing the imbalance and gravity forces in the non-dimensional equations of motion, Eq. (16), it is clear that the influence of gravity decays as inertial effects increase: the non-dimensional gravity force decreases according to $1/n^2$. It is therefore conjectured that a shaft speed exists above which the effect of gravity is unimportant. The magnitudes of the non-dimensional forces are compared in Fig. 14 for an eccentricity of $\epsilon = 0.8(10)^{-4}$ m, over a range of shaft speeds (similar results are obtained for other imbalance magnitudes). At low shaft speeds, the gravitational force dominates the imbalance force: gravity must be included in these regimes to obtain correct results. Once the shaft speed ratio $n/\omega_n = 3$ is reached, the
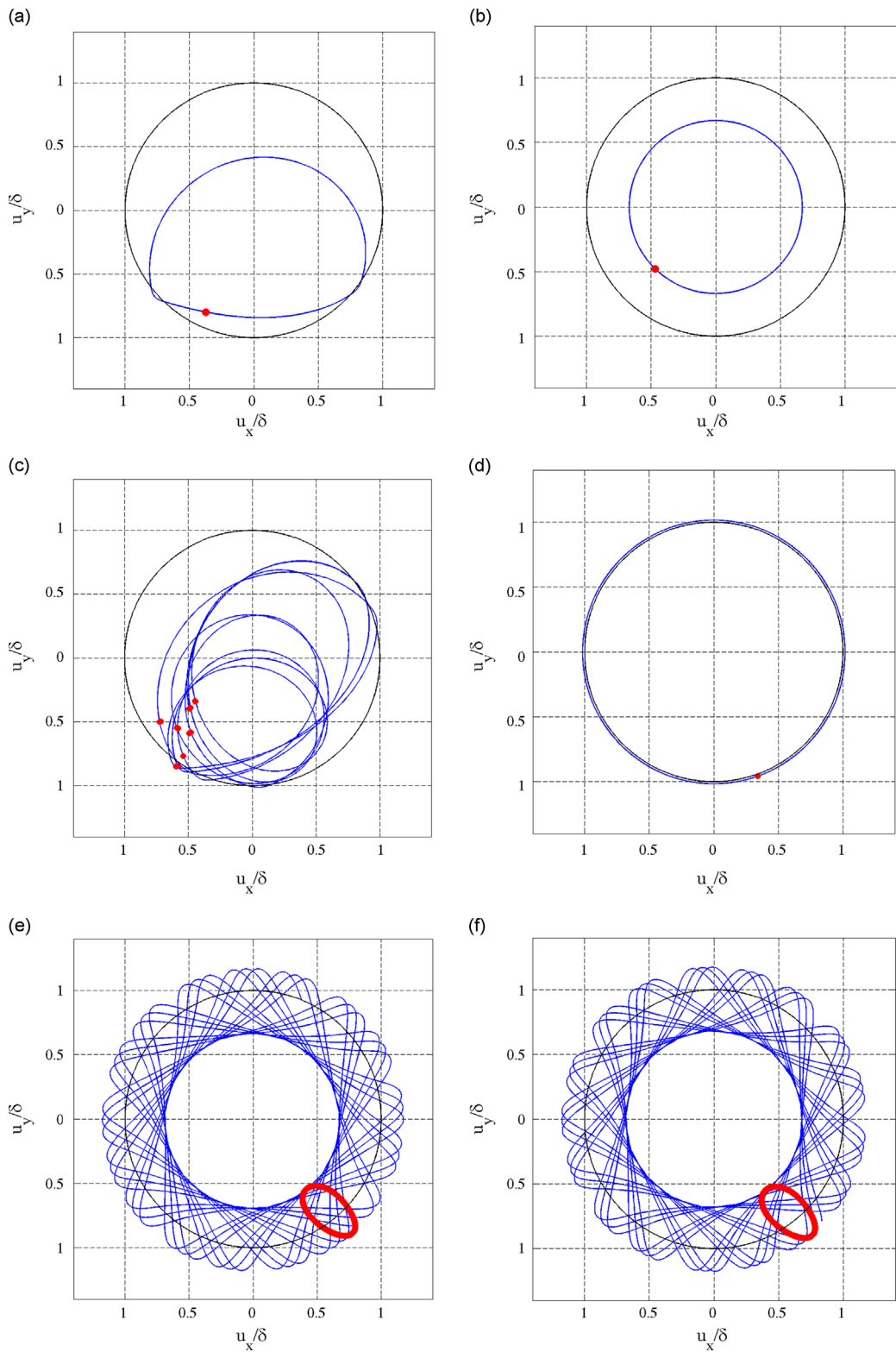
**Fig. 15.** Influence of gravity on dynamic response (symmetric rotor parameter set 2, $c = 4685.2$ N s/m ($\zeta = 0.4277$)). (a) With gravity, $n = 1.5\omega_n$, (b) without gravity, $n = 1.5\omega_n$, (c) with gravity, $n = 2.5\omega_n$, (d) without gravity, $n = 2.5\omega_n$, (e) with gravity, $n = 3.5\omega_n$, and (f) without gravity, $n = 3.5\omega_n$.

magnitude of the gravity force is a full order of magnitude less than that of imbalance; beyond this point, it is hypothesized that gravity can be neglected in the analysis.

These conclusions are corroborated by numeric simulation using symmetric rotor parameter set 2 and a damping coefficient of 4685.2 N s/m (i.e., $\zeta = 0.4277$). When $n = 1.5\omega_n$, the solution with gravity (Fig. 15a) resides in the lower half of the clearance, as expected from intuition. Interestingly, without gravity (Fig. 15b) no contact is observed, thus highlighting the importance of including gravity and imbalance simultaneously. Increasing the shaft speed to $n = 2.5\omega_n$ indicates that gravity is still important (Fig. 15c and d), though inertial effects are beginning to grow, moving the rotor's response partially into the upper portion of the clearance. Still, the responses with and without gravity are dramatically different; the gravity response is period-7, while the no-gravity response is a constrained, fully contacting synchronous response. Once the shaft speed ratio is increased above 3 to $n = 3.5\omega_n$ (the previously conjectured limit above which gravity is unimportant) , the responses with and without gravity are quasiperiodic and indistinguishable (Fig. 15e and f). To neglect gravity in the analysis, the shaft speed range must be chosen appropriately such that inertial effects dominate those due to static deflection.

### 3.3. Influence of asymmetry

Many rotordynamic systems are supported by bearings and fluid film elements with asymmetric and/or cross-coupled stiffness. To the author's knowledge, no previous studies have focused on support asymmetry and its influence on rotor–stator contact, though several studies have incorporated asymmetric fluid film effects [14,24,31]. A study of support asymmetry is important, as worn or improperly designed bearings with asymmetric stiffness may qualitatively change the nature of the nonlinear response to contact. Here, the degree of asymmetry and the importance of cross-coupling stiffness is discussed. All parameter sets referenced in this section are explicitly denoted as belonging to an asymmetric rotor, and can be found in Table A2 of Appendix A.

#### 3.3.1. Cross-coupling stiffness, $k_{xy}$

The influence of the cross-coupling stiffness term $k_{xy}$ on an asymmetrically supported rotor system ($k_{xx} = 1/2 k_{yy}$) is shown in Fig. 16 for asymmetric parameter set 1 (see Table A2 in Appendix A). Fig. 16a provides the rotor's orbit at $n = 2\overline{\omega}_n$
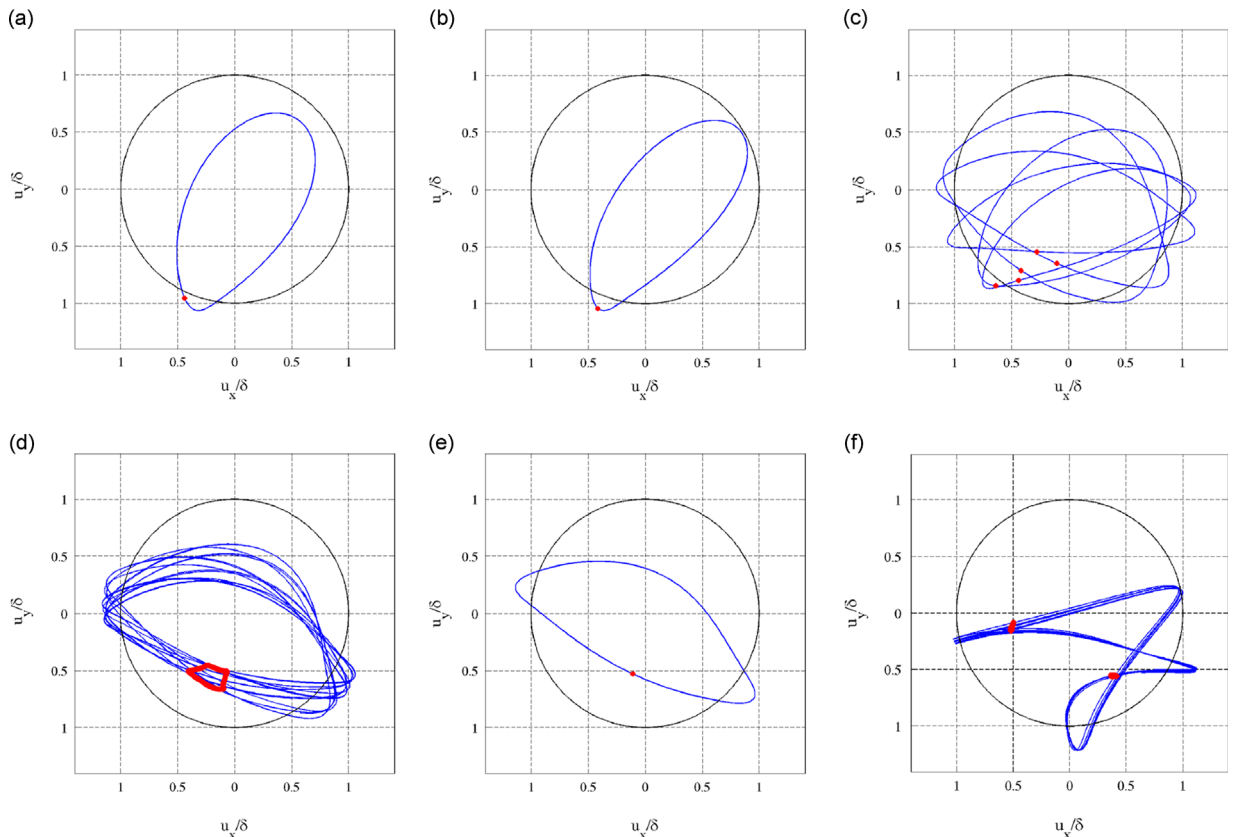


Fig. 16. Influence of cross-coupling stiffness on rotor response (asymmetric rotor parameter set 1, $n = 2\overline{\omega}_n$). (a) $k_{xy} = 0$, (b) $k_{xy} = 1/4 k_{yy}$, (c) $k_{xy} = 1/2 k_{yy}$, (d) $k_{xy} = 4/5 k_{yy}$, (e) $k_{xy} = k_{yy}$, and (f) $k_{xy} = 2 k_{yy}$.
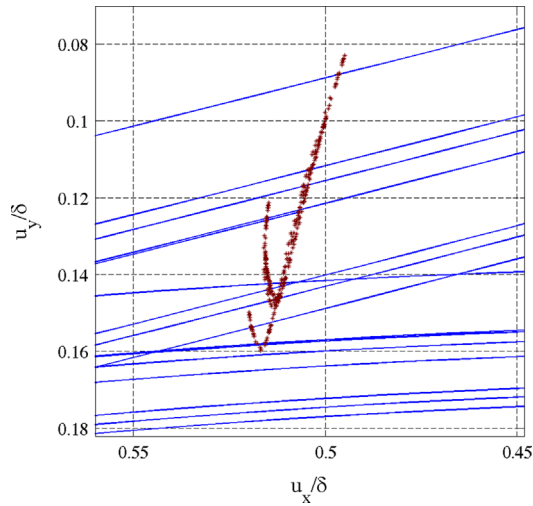
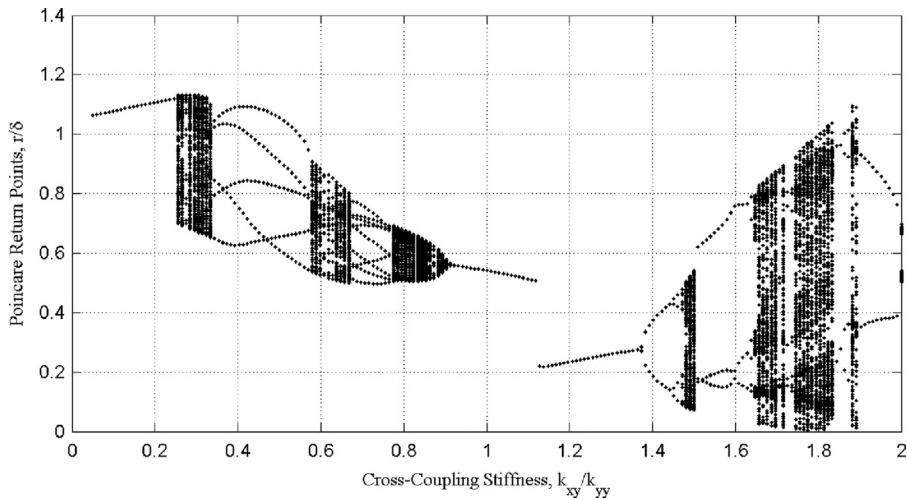Fig. 17. Close view of the chaotic attractor seen in Fig. 16(f).



Fig. 18. Bifurcation diagram with $k_{xy}$ as control parameter (asymmetric rotor parameter set 1).

with zero cross-coupling stiffness; the rotor contacts the stator once per revolution, and the motion is period-1. When the cross-coupling stiffness is increased to one-quarter of the direct stiffness in the $y$-direction, $k_{yy}$, the motion remains period-1 and is qualitatively very similar to the situation with no cross-coupling stiffness. As $k_{xy}$ is increased, a grazing bifurcation occurs in the upper-right quadrant of the clearance, inducing quasiperiodic (Fig. 16d), period-5 (Fig. 16c), and chaotic motions (Fig. 16f). A portion of the Poincaré section (i.e., the chaotic attractor) in Fig. 16f is shown in Fig. 17, where the attractor's complicated and fractal nature is evident. A bifurcation study using the ratio $k_{xy}/k_{yy}$ as the control parameter is given in Fig. 18, where rich bifurcation structure is seen. Period-doubling routes to chaos appear near $k_{xy}/k_{yy}$ ratios of 1.4, 1.6, and 1.9 ($n = 2\overline{\omega}_n$). When the ratio $k_{xy}/k_{yy}$ is less than 0.2, the cross-coupling stiffness does not influence the results significantly; it is concluded that $k_{xy}$ is inconsequential until its magnitude nears that of the direct stiffness terms. For this reason, and to isolate the direct stiffness asymmetry (i.e., $k_{xx} \neq k_{yy}$), this work will assume that cross-coupling stiffnesses are small compared to direct stiffnesses and therefore negligibly impact the response.

### 3.3.2. Direct stiffness asymmetry, $k_{xx} \neq k_{yy}$

Shaft asymmetry is investigated via bifurcation diagrams using the stiffness ratio $k_{xx}/k_{yy}$ and shaft speed as control parameters. In these cases, as discussed previously, cross-coupling stiffness is neglected. Fig. 19 displays the bifurcations of the asymmetrically supported rotor using the stiffness ratio $k_{xx}/k_{yy}$ as a control parameter. Large regions of periodic response are visible, particularly near the stiffness ratio $k_{xx}/k_{yy} = 1$. Small deviations from symmetry can result in drastically different responses, however, indicating the importance of considering support asymmetry. As $k_{xx}$ is increased, a prominent
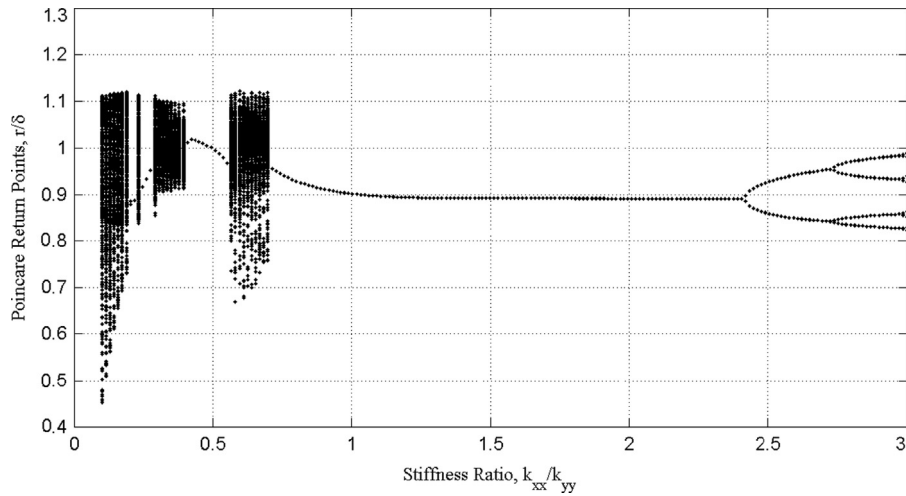
Fig. 19. Bifurcation diagram with $k_{xx}/k_{yy}$ as control parameter (asym. parameter set 2).
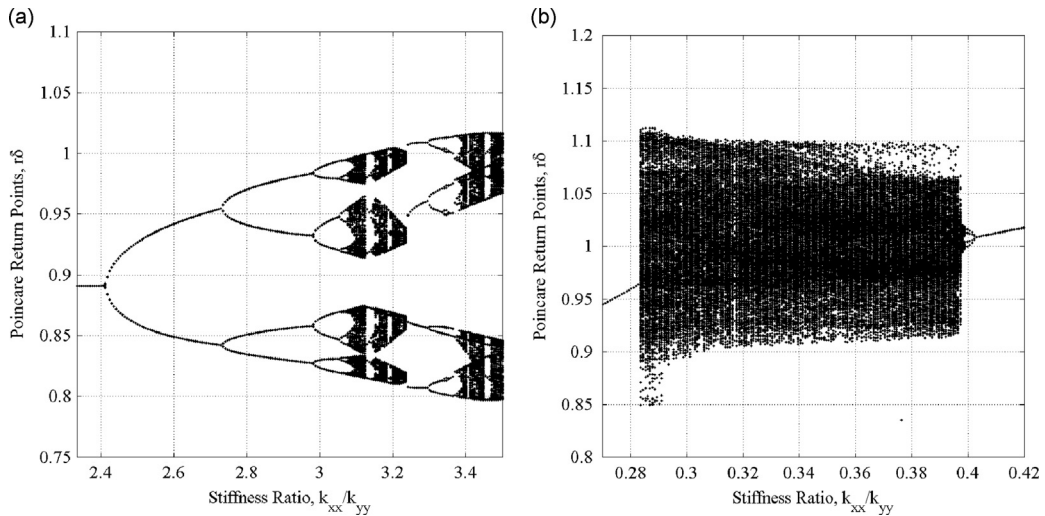


Fig. 20. Routes to chaos in an asymmetric system using $k_{xx}/k_{yy}$ as a control parameter (asymmetric rotor parameter set 2). (a) Period doubling bifurcations and (b) sudden transition to chaos from periodic motion with period-halving exit from chaos.

sequence of period-doubling bifurcations leading to chaos is observed; Fig. 20a gives a detailed view of these phenomena. Chaos is exited following each period-doubling sequence, leading to windows of stability followed by more period-doubling bifurcations to chaos. Another route to chaos evident in Fig. 19 is a sudden transition from periodic motion to chaotic behavior, as detailed in Fig. 20b. Here, a small region of period-halving is observed as a route out of chaos. It must be emphasized that these conclusions hold only for these particular parameters; different combinations of parameters may result in different conclusions.

Direct support stiffness asymmetry is investigated via comparison of the rotor's motion in the orthogonal $x$ and $y$ directions. Hence, the vertical axis in each bifurcation diagram is the Poincaré return points of $u_x$ and $u_y$. Figs. 21 and 22 use $u_x$ and $u_y$ as the Poincaré return points, respectively, while subfigures (a) and (b) in each represent scenarios $k_{yy} = 3k_{xx}$ and $k_{xx} = 3k_{yy}$, respectively. The asymmetric rotor parameter sets referenced in the figures are provided in Table A2 of Appendix A. Observing Fig. 21, it is clear that changing the degree of support asymmetry influences the bifurcation behavior. Fig. 21a displays more prominent period-doubling sequences than Fig. 21b, while the greater $x$-direction stiffness in Fig. 21b restrains the chaotic attractor, resulting in a smaller range of Poincaré return points. These observations are also seen in Fig. 22, when $u_y$ is used as the Poincaré return points. In both cases, a threshold shaft speed near $n/\overline{\omega}_n = 2.5$ is found above which gravity effects are of little consequence, and the rotor's orbit is no longer constrained to predominantly lie in the lower half of the clearance (see Fig. 22, where the Poincaré return points of $u_y$ vary equally between positive and negative values).
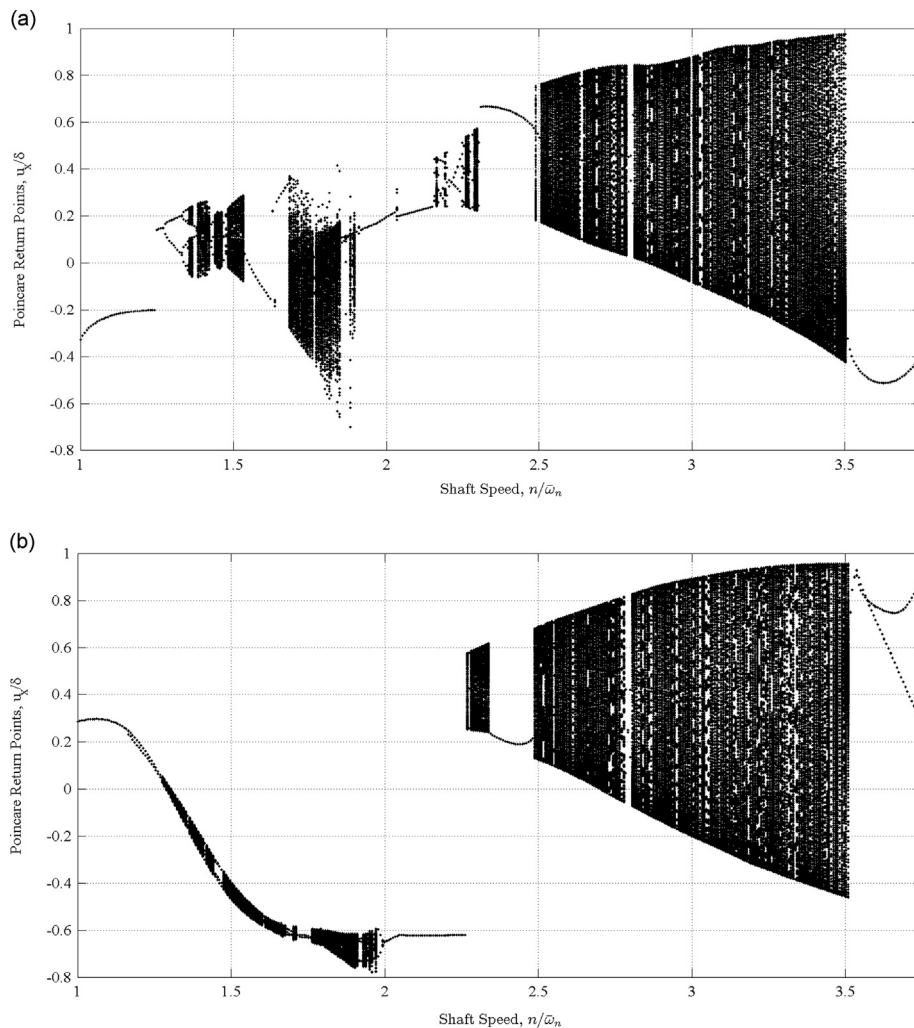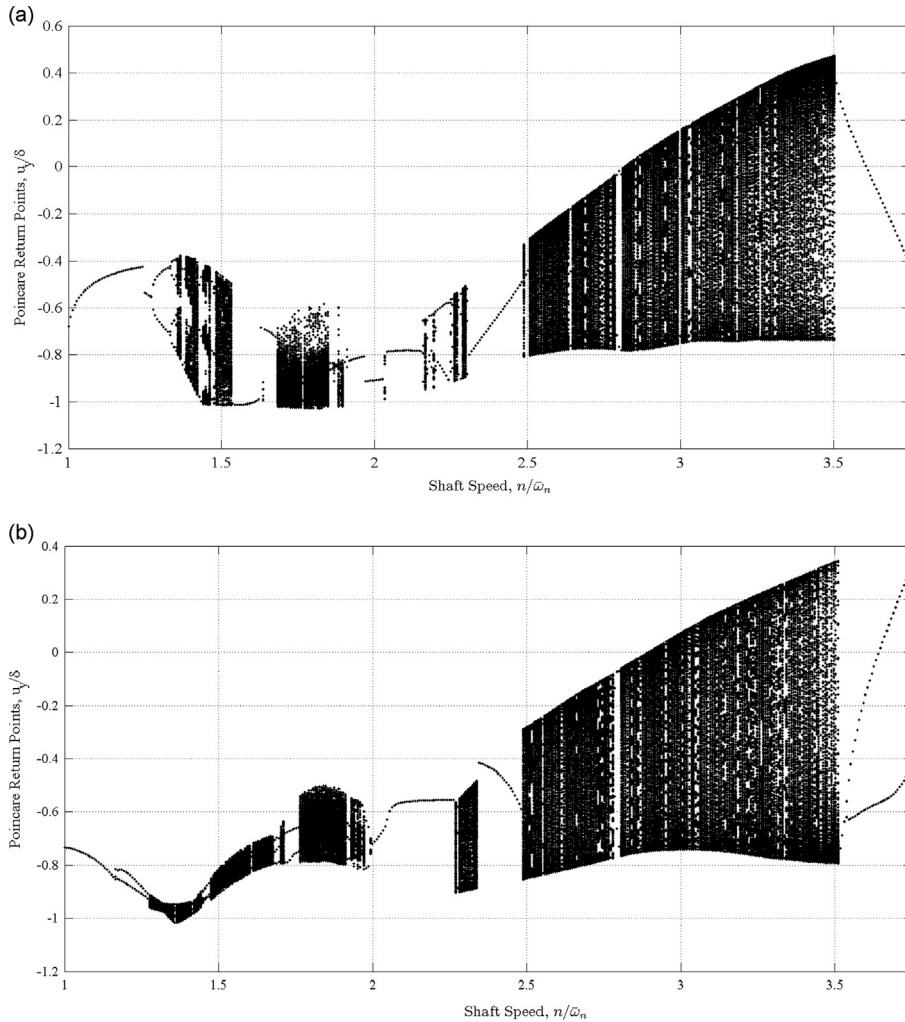
**Fig. 21.** Bifurcation using shaft speed as control parameter (Poincaré return points: $u_x/\delta$). (a) Asymmetric rotor parameter set 3 ($k_{yy} = 3k_{xx}$) and (b) asymmetric rotor parameter set 4 ($k_{xx} = 3k_{yy}$).

## 4. Conclusions

Understanding the nonlinear phenomena associated with rotor–stator contact is important for condition monitoring and the appropriate design of rotating machinery. Adequate design can avoid potentially dangerous and expensive rotor–stator contact, while accurate diagnostics can quickly alert an operator to the presence of rub. To aid in these purposes and further understand the nonlinear phenomena associated with rotor–stator contact, a simple two DOF rotor model has been presented including full asymmetry in the support stiffness matrix. The non-autonomous, strongly nonlinear equations of motion are non-dimensionalized in time and normalized with respect to mass. The coupled nonlinear differential equations are placed in a state-space form suitable for numeric integration. Aspects of the numeric integration are discussed, including numeric stiffness, integration tolerances, and initial conditions.

A wide variety of periodic, quasiperiodic, and chaotic responses are shown for the simple rotor–stator contact system discussed here. The influence of gravity is emphasized, as many authors have neglected gravity in their analysis without due consideration of its effects. A method for ascertaining the threshold shaft speed above which gravity can be neglected is developed, and demonstrated using numeric simulation. Support asymmetry is discussed via bifurcation diagrams involving cross-coupling stiffness, stiffness ratio asymmetry, and shaft speed. The influence of cross-coupling stiffness is negated, as relatively large cross-coupling stiffness coefficients can exist before significantly influencing the results. Direct stiffness asymmetry (i.e., $k_{xx}$ and $k_{yy}$) is shown to strongly influence the results even for small stiffness asymmetries. Period-doubling and sudden bifurcations are seen as the primary routes into chaos, while period-halving is seen as a route out of chaos.

The results emphasize the complexity of such a system, and the need for further work in developing improved models for rotor–stator contact. Extreme sensitivity to small changes in many system parameters highlights the difficulty in

**Fig. 22.** Bifurcation using shaft speed as control parameter (Poincaré return points: $u_y/\delta$). (a) Asymmetric rotor parameter set 3 ($k_{yy} = 3k_{xx}$) and (b) asymmetric rotor parameter set 4 ($k_{xx} = 3k_{yy}$).

successfully predicting even the qualitative nature of the system response. Particular emphasis on model improvement and experiment in the future should focus on a refinement of the rotor–stator interface model, as the current literature provides a broad array of various models with little comparison either analytically or experimentally (e.g., linear versus Hertzian models, impact phenomena, and dry versus viscous friction). Furthermore, contact models and simulation results should be sought for fluid film elements where contact routinely contributes to premature failure, such as non-contacting mechanical face seals.

## Appendix A. Simulation parameters

Parameters used in the symmetric stiffness rotor simulations are provided in Table A1, as referenced throughout the work. If a parameter is not provided, it has been provided in the text (for example, $k_{xy}$ is left out from asymmetric rotor parameter set 1 in Table A2, because various values for this parameter have been used in the text). Parameter sets used in the asymmetrically supported rotor solution are given in Table A2.

**Table A1**
Symmetric rotor parameter sets.

| Parameter | PS1 | PS2 | PS3 | PS4 | PS5 | PS6 |
|-----------|-----|-----|-----|-----|-----|-----|
| $m$ (kg) | 15 | 15 | 5 | 15 | 15 | 5 |
| $k$ (N/m) | $2.0(10)^6$ | $2.0(10)6$ | $1.0(10)6$ | $2.0(10)6$ | $2.0(10)6$ | $2.0(10)6$ |
| $c$ (N s /m) ($\zeta$) | (see below) | (see below) | 1341.6 (0.3) | 3834.1 (0.35) | 3834.1 (0.35) | 2529.8 (0.4) |
| $\epsilon$ (m) | $5.0(10)-5$ | $8.0(10)-5$ | $4.0(10)-5$ | $5.0(10)-5$ | $4.0(10)-5$ | $8.0(10)-5$ |
| $\delta$ (m) | $9(10)-5$ | $1.5(10)-4$ | $9.0(10)-5$ | $9.0(10)-5$ | $9.0(10)-5$ | $1.5(10)-4$ |
| $\mu$ | 0.25 | 0.15 | 0.2 | 0.25 | 0.25 | 0.2 |
| ~~$k_c/k$~~ | 20 | 20 | 20 | 20 | 20 | 32.34 |

**Table A2**
Asymmetric rotor parameter sets.

| Parameter | PS1 | PS2 | PS3 | PS4 |
|-----------|-----|-----|-----|-----|
| $m$ (kg) | 5 | 5 | 1 | 1 |
| $k_{xx}$ (N/m) | $0.5(10)^6$ | $1.0(10)^5$ | $1.0(10)^5$ | $3.0(10)^5$ |
| $k_{yy}$ (N/m) | $1.0(10)^6$ | $1.0(10)^6$ | $3.0(10)^5$ | $1.0(10)^5$ |
| $k_{xy}$ (N/m) | (see below) | 0 | 0 | 0 |
| $c$ (N s/m) ($\zeta$) | 1908.6 (0.5) | 1177.3 (0.4) | 302.4 (0.35) | 302.4 (0.35) |
| $\epsilon$ (m) | $5.0(10)^{-5}$ | $5.0(10)^{-5}$ | $6.0(10)^{-5}$ | $6.0(10)^{-5}$ |
| $\delta$ (m) | $9(10)^{-5}$ | $9.0(10)^{-5}$ | $1.2(10)^{-4}$ | $1.2(10)^{-4}$ |
| $\mu$ | 0.2 | 0.2 | 0.2 | 0.2 |
| $k_c$ (N m) | $100k_{xx}$ | $100k_{yy}$ | $2.0(10)^8$ | $2.0(10)^8$ |

# References

[1] B.L. Newkirk, Shaft rubbing, *Mechanical Engineering* 48 (1926) 830.
[2] A.D. Dimarogonas, A study of the newkirk effect in turbomachinery, *Wear* 28 (1974) 369–382.
[3] W. Kellenberger, Spiral vibrations due to the seal rings in turbogenerators thermally induced interaction between rotor and stator, *Journal of Mechanical Design* 102 (1980) 177–184.
[4] R.F. Beatty, Differentiating rotor response due to radial rubbing, *Journal of Vibration, Acoustics, Stress, and Reliability in Design* 107 (1985) 151–160.
[5] A.S. Lee, I. Green, Higher harmonic oscillations in a non-contacting fmr mechanical face seal test rig, *Journal of Vibration and Acoustics* 116 (1994) 161–167.
[6] F.K. Choy, J. Padovan, Nonlinear transient analysis of rotor-casing rub events, *Journal of Sound and Vibration* 113 (1987) 529–545.
[7] P. Goldman, A. Muszynska, Dynamic effects in mechanical structures with gaps and impacting: order and chaos, *Journal of Vibration and Acoustics* 116 (1994) 541–547.
[8] A. Muszynska, P. Goldman, Chaotic responses of unbalanced rotor/bearing/stator systems with looseness or rubs, *Chaos, Solitons, and Fractals* 5 (1995) 1683–1704.
[9] G.X. Li, M.P. Paidoussis, Impact phenomena of rotor-casing dynamical systems, *Nonlinear Dynamics* 5 (1994) 53–70.
[10] Q.S. Lu, Q.H. Li, E.H. Twizell, The existence of periodic motions in rub-impact rotor systems, *Journal of Sound and Vibration* 264 (2003) 1127–1137.
[11] D.W. Childs, Fractional-frequency rotor motion due to nonsymmetric clearance effects, *ASME Journal of Energy and Power* 104 (1982) 533–541.
[12] Y.B. Kim, S.T. Noah, Bifurcation analysis for a modified Jeffcott rotor with bearing clearances, *Nonlinear Dynamics* 1 (1990) 221–241.
[13] F. Chu, Z. Zhang, Bifurcation and chaos in a rub-impact Jeffcott rotor system, *Journal of Sound and Vibration* 210 (1997) 1–18.
[14] F. Chu, Z. Zhang, Periodic quasi-periodic and chaotic vibrations of a rub-impact rotor system supported on oil film bearings, *International Journal of Engineering Science* 35 (1997) 963–973.
[15] J.T. Sawicki, J. Padovan, R. Al-Khatib, The dynamics of rotor with rubbing, *International Journal of Rotating Machinery* 5 (1999) 295–304.
[16] S. Edwards, A.W. Lees, M.I. Friswell, The influence of torsion on rotor/stator contact in rotating machinery, *Journal of Sound and Vibration* 225 (1999) 767–778.
[17] B.O. Al-Bedoor, Transient torsional and lateral vibrations of unbalanced rotors with rotor-to-stator rubbing, *Journal of Sound and Vibration* 229 (2000) 627–645.
[18] F. Lin, M.P. Schoen, U.A. Korde, Numerical investigation with rub-related vibration in rotating machinery, *Journal of Vibration and Control* 7 (2001) 833–848.
[19] F. Chu, W. Lu, Determination of the rubbing location in a multi-disk rotor system by means of dynamic stiffness identification, *Journal of Sound and Vibration* 248 (2001) 235–246.
[20] E.V. Karpenko, M. Wiercigroch, M.P. Cartmell, Regular and chaotic dynamics of a discontinuously nonlinear rotor system, *Chaos, Solitons, and Fractals* 13 (2002) 1231–1242.
[21] W. Qin, G. Chen, G. Meng, Nonlinear responses of a rub-impact overhung rotor, *Chaos, Solitons, and Fractals* 19 (2004) 1161–1172.
[22] Z.K. Peng, F.L. Chu, P.W. Tse, Detection of the rubbing-caused impacts for rotor–stator fault diagnosis using reassigned scalogram, *Mechanical Systems and Signal Processing* 19 (2005) 391–409.
[23] W.M. Zhang, G. Meng, Stability, bifurcation and chaos of a high-speed rub-impact rotor system in mems, *Sensors and Actuators* 127 (2006) 163–178.
[24] C.W. Chang-Jian, C.K. Chen, Chaos of rub-impact rotor supported by bearings with nonlinear suspension, *Tribology International* 42 (2009) 426–439.
[25] J.I. Inayat-Hussain, Bifurcations in the response of a jeffcott rotor with rotor-to-stator rub, *ASME 2010 Biennial Conference on Engineering Systems Design and Analysis*, Istanbul, Turkey.
[26] T. Yong-Wei, Y. Jiang-Gang, Research on vibration induced by the coupled heat and force due to rotor-to-stator rub, *Journal of Vibration and Control* 17 (2010) 549–566.

[27] J. Cao, C. Ma, Z. Jiang, S. Liu, Nonlinear dynamic analysis of fractional order rub-impact rotor system, *Communications in Nonlinear Science and Numerical Simulation* 16 (2011) 1443–1463.
[28] I. Abu-Mahfouz, A. Banerjee, On the investigation of nonlinear dynamics of a rotor with rub-impact using numerical analysis and evolutionary algorithms, *Procedia Computer Science* 20 (2013) 140–147.
[29] T.H. Patel, A.K. Darpe, Study of coast-up vibration response for rub detection, *Mechanism and Machine Theory* 44 (2009) 1570–1579.
[30] Z.C. Feng, X.Z. Zhang, Rubbing phenomena in rotor–stator contact, *Chaos, Solitons, and Fractals* 14 (2002) 257–267.
[31] C.W. Chang-Jian, C.K. Chen, Chaos and bifurcation of a flexible rub-impact rotor supported by oil film bearings with nonlinear suspension, *Mechanism and Machine Theory* 42 (2007) 312–333.
[32] J.P. Chavez, M. Wiercigroch, Bifurcation analysis of periodic orbits of a non-smooth jeffcott rotor model, *Communications in Nonlinear Science and Numerical Simulation* 18 (2013) 2571–2580.
[33] S. Popprath, H. Ecker, Nonlinear dynamics of a rotor contacting an elastically suspended stator, *Journal of Sound and Vibration* 308 (2007) 767–784.
[34] G.V. Groll, D.J. Ewins, A mechanism of low subharmonic response in rotor/stator contact—measurements and simulation, *Journal of Vibration and Acoustics* 124 (2002) 350–358.
[35] Abu-Mahfouz, Routes to Chaos in Rotor Dynamics, PhD thesis, Case Western Reserve University, 1993.
[36] W. Qin, H. Su, Y. Yang, Grazing bifurcation and chaos in response of rubbing rotor, *Chaos, Solitons, and Fractals* 37 (2008) 166–174.
[37] P. Pennacchi, N. Bachschmid, E. Tanzi, Light and short arc rubs in rotating machines: experimental tests and modelling, *Mechanical Systems and Signal Processing* 23 (2009) 2205–2227.
[38] M. Behzad, M. Alvandia, D. Mba, J. Jamali, A finite element-based algorithm for rubbing induced vibration prediction in rotors, *Journal of Sound and Vibration* 332 (2013) 5523–5542.
[39] J. Sawicki, A. Montilla-Bravo, Z. Gosiewski, Thermomechanical behavior of rotor with rubbing, *International Journal of Rotating Machinery* 9 (2003) 41–47.
[40] X. Dai, Z. Jin, X. Zhang, Dynamic behavior of the full rotor/stop rubbing: *numerical simulation and experimental verification*, *Journal of Sound and Vibration* 251 (2002) 807–822.
[41] Z. Yuan, F. Chu, R. Hao, Simulation of rotor's axial rub-impact in full degrees of freedom, *Mechanism and Machine Theory* 42 (2007) 763–775.
[42] T.H. Patel, A.K. Darpe, Coupled bending-torsional vibration analysis of rotor with rub and crack, *Journal of Sound and Vibration* 326 (2009) 740–752.
[43] D. Bently, Forced subrotative speed dynamic action of rotating machinery, *Petroleum Mechanical Engineering Conference*, Dallas, TX.
[44] F. Ehrich, Observations of subcritical superharmonic and chaotic response in rotordynamics, *Journal of Vibration and Acoustics* 114 (1992) 93–100.
[45] Y.S. Choi, S.T. Noah, Nonlinear steady-state response of a rotor-support system, *ASME Journal of Vibration, Acoustics, Stress, and Reliability in Design* 109 (1987) 255–261.
[46] M.J. Feigenbaum, Quantitative universality for a class of nonlinear transformations, *Journal of Statistical Physics* 19 (1978) 25–52.
[47] J.D. Jeng, Y. Kang, Y.P. Chang, An alternative poincare section for high-order harmonic and chaotic responses of a rubbing rotor, *Journal of Sound and Vibration* 328 (2009) 191–202.
[48] J. Yu, On occurrence of reverse full annular rub, *ASME Journal of Engineering for Gas Turbines and Power* 134 (2012) 219–227.
[49] J.J. Yu, P. Goldman, D.E. Bently, A. Muzynska, Rotor/seal experimental and analytical study on full annular rub, *ASME Journal of Engineering for Gas Turbines and Power* 124 (2002) 340–350.
[50] J.J. Yu, Rub diagnostics based on vibration data, *ASME Turbo Expo*, San Antonio, TX.
[51] T.H. Patel, A.K. Darpe, Vibration response of a cracked rotor in presence of rotor–stator rub, *Journal of Sound and Vibration* 317 (2008) 841–865.
[52] T.H. Patel, M.J. Zuo, A.K. Darpe, Vibration response of coupled rotor systems with crack and misalignment, *Proceedings of the Institution of Mechanical Engineers, Part C: Journal of Mechanical Engineering Science* 225 (2011) 700–713.
[53] W. Fengqi, G. Meng, Compound rub malfunctions feature extraction based on full-spectrum cascade analysis and SVM, *Mechanical Systems and Signal Processing* 20 (2006) 2007–2021.
[54] P. Goldman, A. Muszynska, Application of full spectrum to rotating machinery diagnostics, *Bentley Nevada Orbit* 1 (1999) 17–21.
[55] K. Qi, Z. He, Y. Zi, Cosine window-based boundary processing method for emd and its application in rubbing fault diagnosis, *Mechanical Systems and Signal Processing* 21 (2007) 2750–2760.
[56] J. Cheng, D. Yu, J. Tang, Y. Yang, Local rub-impact fault diagnosis of the rotor systems based on emd, *Mechanism and Machine Theory* 44 (2009) 784–791.
[57] C.W. Lee, *Vibration Analysis of Rotors*, Kluwer Academic Publishers, Boston, 1993.
[58] P. Thota, H. Dankowicz, Tc-hat: a novel toolbox for the continuation of periodic trajectories in hybrid dynamical systems, *SIAM Journal of Applied Dynamical Systems* 7 (2008) 1283–1322.
[59] A.H. Nayfeh, B. Balachandran, *Applied Nonlinear Dynamics: Analytical, Computational, and Experimental Methods*, Wiley-VCH, Weinheim, Germany, 2004.
[60] J.K. Hale, *Oscillations in Nonlinear Systems*, McGraw-Hill, New York, 1963.
[61] M. Urabe, Quasiperiodic solutions of ordinary differential equations, *Nonlinear Vibration Problems* 18 (1974) 85–93.